

SUPPORTING INFORMATION

Controlled Anisotropic Growth of Hydroxyapatite by Additive-Free Hydrothermal Synthesis

Jordi Sans,^{1,2} Vanesa Sanz,³ Jordi Puiggali,^{1,2,4} Pau Turon,^{3,} and Carlos Alemán^{1,2,4*}*

¹ Departament d'Enginyeria Química, EEBE, Universitat Politècnica de Catalunya, C/

Eduard Maristany, 10-14, Ed. I2, 08019, Barcelona, Spain

² Barcelona Research Center in Multiscale Science and Engineering, Universitat Politècnica de Catalunya, C/ Eduard Maristany, 10-14, 08019, Barcelona, Spain

³ B. Braun Surgical, S.A. Carretera de Terrasa 121, 08191 Rubí (Barcelona), Spain

⁴ Institute for Bioengineering of Catalonia (IBEC), The Barcelona Institute of Science and Technology, Baldiri Reixac 10-12, 08028 Barcelona Spain

Page	Description
S2-S3	Materials and characterization methods
S4	Figure S1. FTIR spectra for samples s1-s4.
S4	Figure S2. Raman spectra for samples s1-s4.
S5	Figure S3. FTIR spectra, Raman spectra and WAXS patterns for samples s5-s10.
S5	Figure S4. WAXS diffractograms for samples s14 and s15.
S6	Figure S5. Variation of the $I_{002/211}$ ratio with the final pH for samples prepared using 100 and 500 mM $\text{Ca}(\text{NO}_3)_2$ ethanol solutions

EXPERIMENTAL METHODS

Materials

Calcium nitrate [Ca(NO₃)₂], diammonium hydrogen phosphate [(NH₄)₂HPO₄; purity > 99.0%] and ammonium hydroxide solution 30% [NH₄OH; purity 28-30% w/w] were purchased from Sigma Aldrich. Ethanol (purity > 99.5%) was purchased from Scharlab. All experiments were performed with milli-Q water.

Characterization of the samples

Structural fingerprint was obtained using the inVia Qontor confocal Raman microscope (Renishaw) with a resolution of 100 nm in the X,Y-axes, equipped with a Renishaw Centrus 2957T2 detector and using both a 785 nm and a 532 nm laser for enhancing lower and higher regions of the Raman shift, respectively. The images were obtained focusing the laser to a bunch of rods (using the ×100 objective) and careful control of the focusing beam onto the surface of the sample using LiveTrack Measurements options available in the software of the equipment. Due to the size and the clear differences between rods and plates in the micrometric scale, the two different spectra could be obtained. Other advance set up parameters like the use of a pinhole was chosen to refine the quality of the laser in the desired area of analysis.

Vibrational studies were completed using FTIR spectroscopy. Spectra were recorded on a FTIR Jasco 4100 spectrophotometer through an attenuated total reflection accessory (Top-plate) with a diamond crystal (Specac model MKII Golden Gate Heated Single Reflection Diamond ATR). Samples were evaluated using spectra manager software and, for each sample 64 scans were performed between 4000 and 600 cm⁻¹ with a resolution of 4 cm⁻¹.

Wide angle X-ray scattering (WAXS) studies were conducted using a Bruker D8 Advance model with Bragg-Brentano 2θ configuration and Cu K_α radiation ($\lambda = 0.1542$ nm). Measurements were performed in a 2θ range of $20^\circ - 60^\circ$ in steps of 0.02° , and scan speed of 2 s using a one-dimensional Lynx Eye detector. The crystallinity (χ_c) was obtained using the following expression:^{S1}

$$\chi_c = 1 - \frac{V_{112/300}}{I_{300}} \quad (\text{S1})$$

where I_{300} is the intensity of the (300) reflection and $V_{112/300}$ is the intensity of the hollow between the (112) and (300) reflections, which disappears in non-crystalline samples. The crystallite size, L_{hkl} , was calculated using the Debye-Scherrer equation

$$L_{hkl} = \frac{0.9 \cdot \lambda}{B \cdot \cos \theta_{hkl}} \quad (\text{S2})$$

where λ is the wavelength of the monochromatic X-ray beam, B is the full width at half maximum of the peak at the maximum intensity, and θ_{hkl} is the peak diffraction angle that satisfies the Bragg's law for the (hkl) plane.

Morphological characterization has been performed by scanning electron microscopy (SEM) using a Focused Ion Beam Zeiss Neon40 microscope equipped with a SEM GEMINI column with a Shottky field emission. Samples were sputter-coated with a thin layer of carbon to prevent sample charging problems.

S1. Landi, E.; Tampieri, A.; Celotti, G.; Sprio, S. Densification Behavior and Mechanisms of Synthetic Hydroxyapatite. *J. Eur. Ceram. Soc.* **2000**, *20*, 2377–2387.

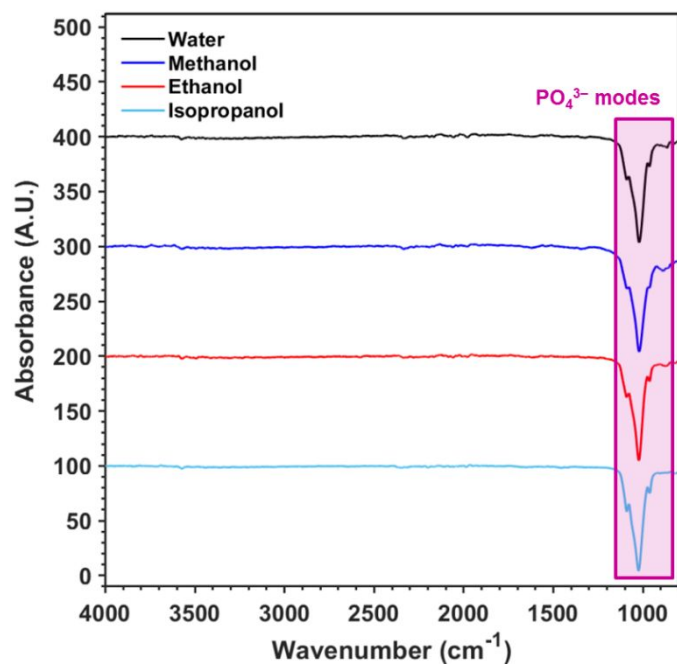


Figure S1. FTIR spectra of samples prepared using a 100 mM $\text{Ca}(\text{NO}_3)_2$ solution with different solvents at pH 10.5 (s1-s4 in Table 1).

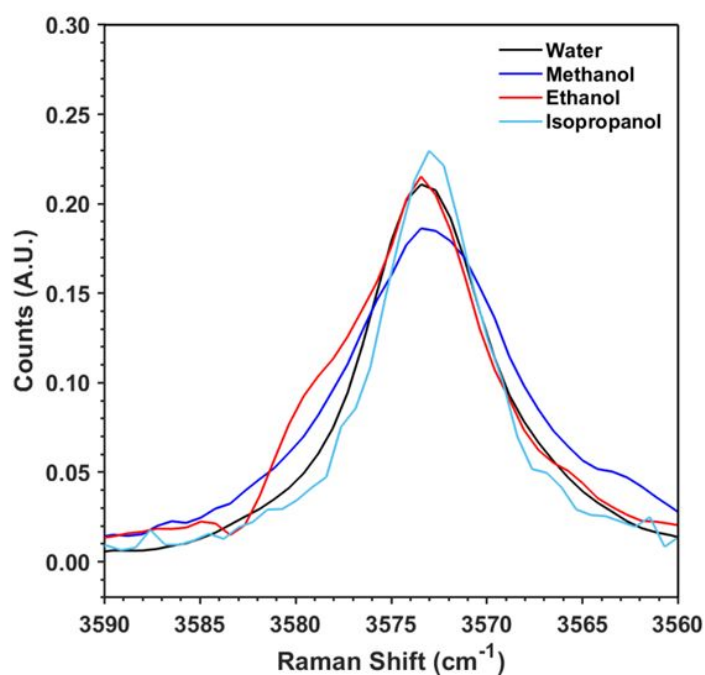


Figure S2. Raman spectra in the 3560–3590 cm^{-1} region for samples prepared using 100 mM $\text{Ca}(\text{NO}_3)_2$ solutions with different solvents at pH 10.5 (s1-s4 in Table 1). The intensity of the peak at 3573 cm^{-1} is related with the amount of OH^- in the HAp crystal lattice. Spectra were recorded using the 532 nm laser.

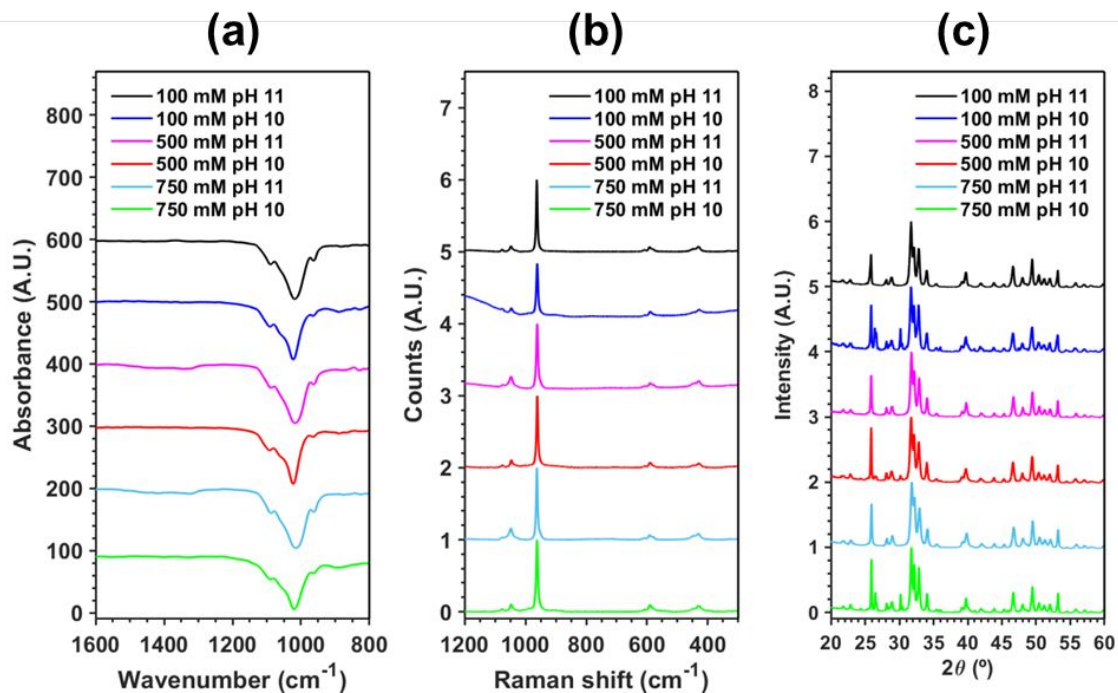


Figure S3. (a) FTIR spectra, (b) Raman spectra and (c) WAXS patterns for samples s5-s10 (Table 1).

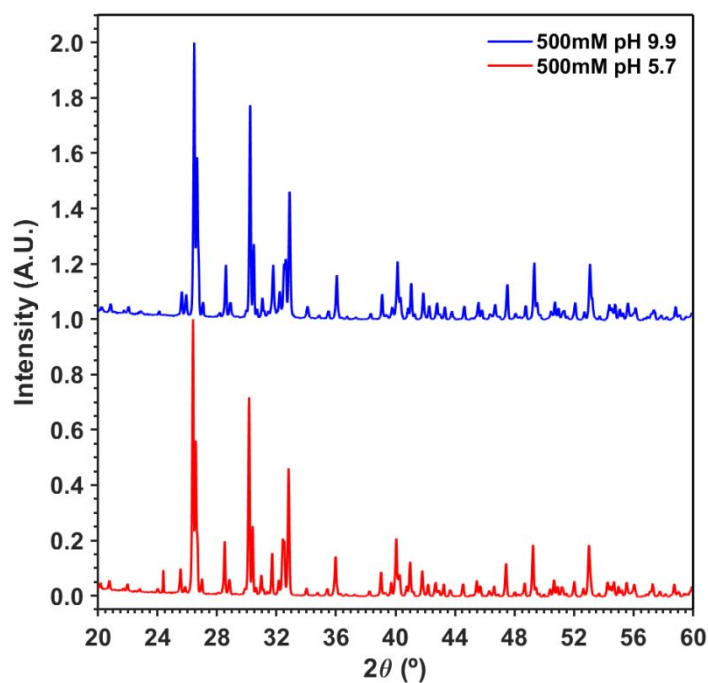


Figure S4. WAXS diffractograms for samples s14 and s15 (Table 1).

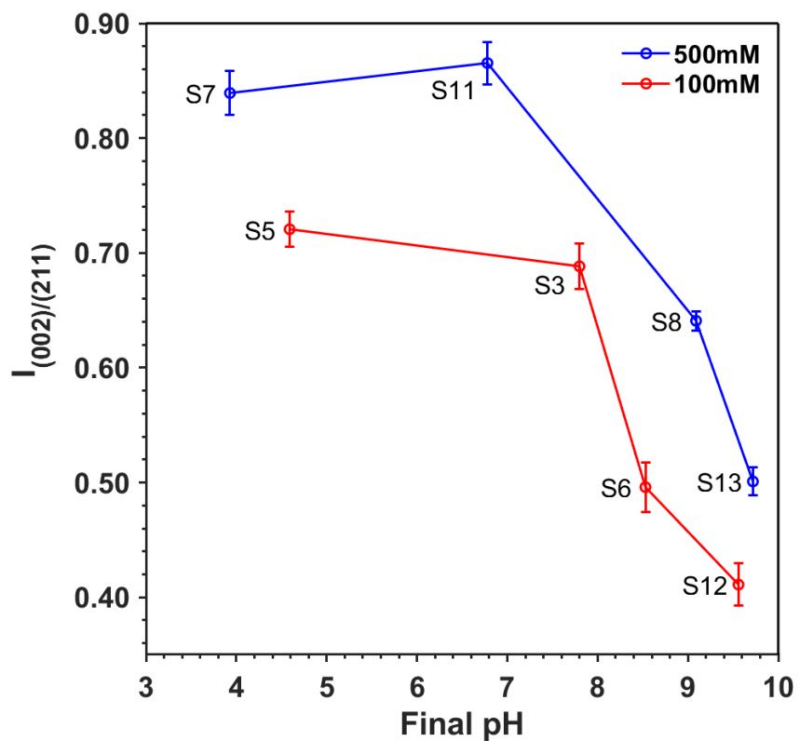


Figure S5. Variation of the $I_{002/211}$ ratio, as determined from WAXS diffractograms, with the pH for samples prepared using 100 and 500 mM $\text{Ca}(\text{NO}_3)_2$ ethanol solutions. The difference between this representation and that displayed in Figure 5, in which the pH is that adjusted for the $\text{Ca}(\text{NO}_3)_2$ ethanol solution, is that in this case the pH corresponds to the final mixture of the $\text{Ca}(\text{NO}_3)_2$ ethanol and $(\text{NH}_4)_2\text{HPO}_4$ aqueous solutions.